Chemical Vapor Deposition

DOI: 10.1002/cvde.201407139

Full Paper

Doped Polycrystalline Silicon Thin Films Deposited on Glass from Trichlorosilane**

By *Ariel G. Benvenuto, Román H. Buitrago,* and *Javier A. Schmidt**

Atmospheric pressure (AP) thermal CVD is used to deposit thin poly-Si films on glass substrates. Also produced are heterojunction solar cells carrying out the deposition on c-Si wafers. A batch-type hot-wall reactor, employing $SiHCl_3$ as a precursor, H_2 as a carrier and reaction gas, BBr_3 as a *p*-type doping agent, and PCl_3 as a *n*-type doping agent, is used. The films obtained are homogeneous and well-adhered to the substrate. Samples are structurally characterized by scanning electron microscopy (SEM), atomic force microscopy (AFM), reflectance spectroscopy in the UV-vis region, X-ray diffraction (XRD), and Raman spectroscopy (RS). The electrical characterization includes conductivity measurements as a function of temperature, and Hall effect measurements. For the *p*-doped samples, XRD reveals a strong (220) preferential orientation of the films, while the *n*-doped samples lack columnar structure or preferential orientation. RS and UV-reflectance confirm a high crystalline fraction. Dark conductivity measurements as a function of temperature show that the films can be grown intrinsic, *p*-type or *n*-type. Activation energies between 0.61 and ~0 eV are obtained, with reasonable values for the carrier mobilities. For the solar cells, relatively high values of V_{OC}(~507 mV) and J_{SC} (~29.6 mA cm^{-2}) are measured. In conclusion, these results demonstrate the feasibility of directly depositing doped poly-Si thin films on glass and c-Si substrates at intermediate temperatures, with interesting characteristics for photovoltaic applications.

Keywords: CVD-based deposition, Polycrystalline silicon, Solar cells, Thin film characterization

1. Introduction

Thin film polycrystalline silicon (poly-Si) solar cells deposited on low-cost substrates may be the path to achieve the expected reduction in the price of photovoltaic electricity. Poly-Si could combine, in principle, the low-cost potential of thin films with the proven stability and high efficiency of crystalline silicon.

Having in mind the objective of using low-cost reactants and processes, we have chosen APCVD as the deposition method. APCVD provides high deposition rates, acceptable uniformity, controllable doping profiles, and good film quality, with a relatively simple set-up.[1,2] As substrates, we use commercial float glass or crystalline silicon wafers. The glass we use is Schott AF37, which, in addition to withstanding the process temperature (less than 850 °C), has a thermal expansion coefficient closely matching that of crystalline silicon.[3] The Si wafers are (100)-oriented *p*-type Czochralski c-Si, and act as the base of the cell. As a silicon source we use trichlorosilane ($SiHCl_3$, TCS), which can be obtained by hydrochlorination of metallurgical-grade silicon, and can be easily purified by distillation.[4] The deposition of thin film silicon on float glass by APCVD from TCS at intermediate temperatures has not previously been explored. Other authors have used APCVD from TCS,[1,5,6] but at temperatures higher than 900 °C, thus limiting, to ceramics or low-cost silicon, the substrates that can be used. The use of float glass substrates can potentially reduce the cost of the solar cells, offering also the possibility of depositing them in a superstrate configuration. Moreover, the use of temperatures lower than 850 °C points towards lowering the energy budget of the process. The material saving due to the use of thin films, in addition to the lower deposition temperatures required, would lead to a reduction of costs compared to bulk polycrystalline silicon solar cells. Using glass as the substrate, the APCVD process should be scalable to a size comparable to that of the amorphous silicon solar panels currently manufactured, and the monolithic interconnection of the modules would also lead to a reduction in the manufacturing costs.

In previous works, we have shown that intrinsic poly-Si layers, exhibiting good structural and optical properties, can be deposited by APCVD on glass substrates.[7,8] The next step towards the production of solar cells is the deposition of doped layers. For that reason, in this work we study the electrical, optical, and structural properties of poly-Si samples doped with both B and P. In the case of *p*-doped samples we explore the possibility of depositing both lightly and heavily doped materials, which could act as the base and

[*] Dr. A. G. Benvenuto, Dr. R. H. Buitrago, Dr. J. A. Schmidt
Instituto de Física del Litoral (IFIS-Litoral), Guemes 3450 S3000GLN, Santa Fe, Argentina
E-mail: javier.schmidt@santafe-conicet.gov.ar

[**] This research was supported by ANPCyT (Projects 22-32515 and 22-25749), CONICET (Project PIP 1464) and UNL (Project CAI + D 68-349)

the back surface field of a solar cell, respectively. For *n*-doped samples we try to achieve the doping level needed for the emitter of a solar cell (n^+ layer). Finally, we explore the concept of a heterojunction solar cell between a *p*-type c-Si base and an n^+ poly-Si emitter.

2. Results and Discussion

The global chemical reactions leading to silicon, boron, and phosphorous deposition can be written $SiHCl_3(g) + H_2(g) \overset{\Delta}{\longleftrightarrow} Si(s) + 3HCl(g)$,
$2BBr_3(g) + 3H_2(g) \overset{\Delta}{\rightarrow} 2B(s) + 6HBr(g)$, and
$2PCl_3(g) + 3H_2(g) \overset{\Delta}{\rightarrow} 2P(s) + 6HCl(g)$.

TLS reduces at high temperature in the presence of hydrogen, resulting in the deposition of silicon and the release of hydrochloric acid. This reaction is reversible, meaning that, under certain circumstances, hydrogen chloride can etch the silicon deposited.[7] Boron tribromide or phosphorous trichloride also reduce in the presence of hydrogen, leading to the incorporation of boron or phosphorous into the silicon lattice, and the release of hydrobromic or hydrochloric acid, respectively.

2.1. Boron-doped Samples

2.1.1. Electrical Properties

By adjusting the temperature of BBr_3, different B concentrations have been incorporated into the poly-Si samples. Knowing the vapor pressure of $SiHCl_3$ at 0 °C and of BBr_3 at the various temperatures, and taking into account the hydrogen flows into both liquids, the ratio of boron to silicon atoms in the gas phase, *R*, has been calculated. Figure 1 shows the room temperature resistivity of the samples as a function of *R*. As can be seen, the resistivity is $\sim 1.3 \times 10^5$ Ω cm for the nominally intrinsic sample. The addition of a small amount of boron leads to an increase of the resistivity, which reaches a maximum value of $\sim 5 \times 10^6$ Ω cm. This is evidence that the nominally intrinsic samples are slightly *n*-type. Other groups have also reported that films produced with no intentionally added dopants were *n*-type.[9] This *n*-type characteristic is suggested to be possibly caused by diffusion of impurities from the substrate or other layers, or by oxygen contamination.[10,11] Under certain circumstances, oxygen may form complicated multi-atom centers in silicon, called "thermal donors", which act as electrically active donor states, that is, as *n*-type dopants.[12] In the work of Angermeier et al.,[13] resistivities of about 20 Ω cm are reported for non-intentionally doped poly-Si layers grown on graphite substrates. The large resistivities measured for our intrinsic samples are an indication of the absence of substantial contamination in the deposition system that we use. Moreover, we performed an electron probe micro-analysis (EPMA) of the sample without observing signs of contamination within the limits of detection of our equipment.

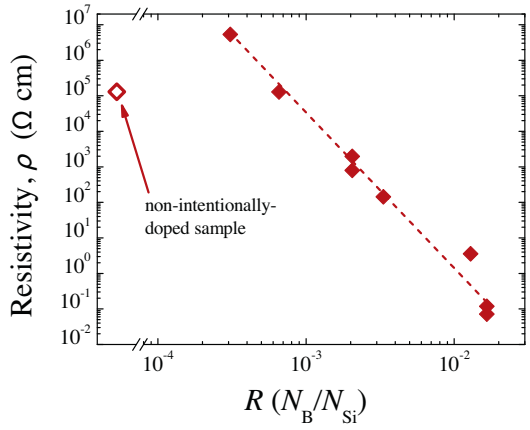

Fig. 1. Room temperature resistivity as a function of the ratio of boron to silicon atoms in the gas phase, *R*. The first point to the left corresponds to the nominally intrinsic sample. The line is a guide to the eye.

A further increase in the boron content leads to *p*-doped samples, with resistivities that gradually decrease to a value as low as 0.07 Ω cm. An increase of less than two orders of magnitude in *R* causes a decrease of almost eight orders of magnitude in resistivity, making clear the large influence of doping. The dark conductivity activation energy exhibits a consistent behavior with that of the resistivity, with a value around 0.5 eV for undoped sample, an increase to about 0.61 eV for the compensated sample, and a further decrease to approximately zero for the heavily boron-doped samples.

We have used Hall effect measurements to study the evolution of the majority carriers concentration and drift mobility as a function of boron concentration. The results confirm that the majority carriers are holes, with concentrations ranging from $p < 10^{14}$ cm^{-3} for the sample deposited with $R = 3 \times 10^{-4}$ (quasi-compensated sample) through $p = 2 \times 10^{17}$ cm^{-3} for $R = 3.3 \times 10^{-3}$ (lightly *p*-doped sample) to $p = 3.4 \times 10^{19}$ cm^{-3} for $R = 1.7 \times 10^{-2}$ (heavily *p*-doped sample, p^+). This last value of *p* is close to the one required for the back surface field of a solar cell. Knowing the concentrations in the gas phase, it is possible to calculate the doping efficiency. $R = 3 \times 10^{-4}$ means that, if the proportion in the gas phase were maintained in the solid, there would be 1.5×10^{19} B atoms per cm^3, however we have measured $p < 10^{14}$ cm^{-3}, meaning that less than one in 1.5×10^5 boron atoms present in the gas phase effectively contributes to the semiconductor with one free hole. This could mean a preferential incorporation of silicon over boron into the solid, but more probably it is due to trapping of holes into defect states, as we will explain. Polycrystalline silicon, especially when it has a small grain size, has a large quantity of defect states in the grain boundaries (N_T traps per unit area).[14] Trapping into these states causes the concentration of free holes to be considerably lower than the concentration of acceptor atoms. When the concentration of acceptors increases, however, the trap states begin

to saturate and the concentration of free holes increases. For $R = 3.3 \times 10^{-3}$ we have measured $p = 3.4 \times 10^{19}$ cm^{-3}, meaning that one in 775 boron atoms present in the gas phase contributes with a free hole, and this proportion changes to 1 in 25 for $R = 1.7 \times 10^{-2}$. This is consistent with the fact that, when the doping concentration increases and traps begin to saturate, the concentration of free holes tends towards the concentration of doping atoms.

In Figure 2, we show the Hall mobility as a function of the holes concentration for the different samples. As can be seen, mobility increases with p from a low value (0.07 cm^2 V^{-1} s^{-1}) for the less-doped sample to ~15 cm^2 V^{-1} s^{-1} for the sample with the highest boron content. A similar trend is seen in the work of Münster et al.,[15] where the authors report mobilities in the range of 6 to 30 cm^2 V^{-1} s^{-1}. The behavior in Figure 2 can also be explained by the presence of a high density of trap states in the grain boundaries. When carriers are trapped the defects acquire electric charge, creating a potential barrier that opposes the movement of carriers between adjacent grains and thus reduces the mobility. For higher doping levels, the carrier concentration is only partially reduced, the barrier height decreases, and the mobility increases.[14,16]

2.1.2. Structural Properties

The thickness of the poly-Si films was calculated from the distance between the peaks of the reflectance spectrum in the range of 400–900 nm. Samples around 4.1 μm thick were grown for this study. The deposition rate was calculated by dividing the thickness by the deposition time (15 min in all cases), assuming that the incubation period is short compared to the total deposition time. The deposition rate was around 0.27 μm min^{-1} in all cases.

SEM was used to explore the front surface and the cross-section of the samples. The grain size and the structure were evaluated from these images. The average grain size is about 190 nm, independent of the BBr_3 concentration. Within the doping range of our experiments, this average grain size is lower than that of undoped samples (around 270 nm) deposited with the same procedure and the same parameters.[7,8] This means that the addition of boron increases the nucleation rate. Depositing boron-doped μc-Si films by plasma-enhanced (PE)CVD from silane and diborane, Toyama et al.[17] reached a similar conclusion. A typical SEM front view of one of the samples can be seen in Figure 3a. AFM images show conical structures with grain dimensions that are compatible with those obtained from SEM observations. The root mean square (rms) roughness, evaluated from the AFM images, is about 11 nm.

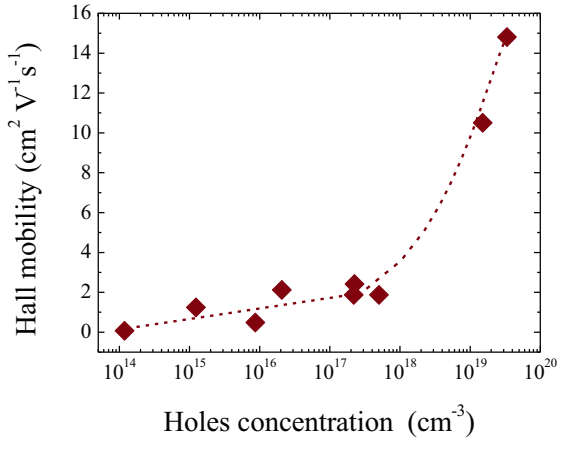

Fig. 2. Hall mobility as a function of hole concentration for p-doped samples. The line is a guide to the eye.

By producing poly-Si thin films with other reactor types, and at higher deposition temperatures (between 1000 and 1200 °C), other groups have obtained larger grain sizes, in the range 1 to 10 μm.[13,18] In those works, higher temperature-resistant materials, such as oxidized silicon, alumina, mullite, and graphite, were used as substrates. This implies a higher thermal budget and possibly higher material costs. Moreover, the non-transparent substrates make production of the cells in the superstrate configuration impossible. Although some authors aim at enlarging the grain size as a direct way of reducing the defect density, photovoltaic cells with an open-circuit voltage of 536 mV have been produced with poly-Si layers having a grain size of 0.1–0.2 μm.[19] This is a demonstration that the relatively small grain size that we obtain should not prevent the attainment of good photovoltaic properties, as long as the intra-grain quality is adequate and the grain boundaries are of low electronic activity.

From Raman scattering spectra we estimated the crystalline fraction of the samples. Contrary to what we have found in intrinsic samples, we observed an amorphous phase contribution for those samples prepared with low doping concentrations. The amorphous contribution comes from the disordered region between grains. The Raman spectra have been fitted with the sum of a Lorentzian function centered at ca. 520 cm^{-1}, representing the crystalline component, a Gaussian function centered at ca. 510 cm^{-1}, corresponding to the nanocrystalline grains, and a Gaussian function centered at ca. 480 cm^{-1} corresponding to the amorphous phase. After that, the crystalline fraction was calculated with the usual formula, Equation 1.

$$X_{\mathrm{C,\ Raman}} = \frac{A_{520} + A_{510}}{A_{520} + A_{510} + \gamma\, A_{480}} \quad (1)$$

A_x are the areas of the related peaks and γ is the ratio between the phonon excitation cross-sections of crystalline silicon and amorphous silicon. For this parameter we adopt the value $\gamma = 0.8$ as in the literature.[20]

The Raman crystalline fraction is shown in Figure 4 (red circles, left scale). For low doping concentrations we can see a decrease of $X_{\mathrm{C,Raman}}$ from the value for the intrinsic sample,

Chemical Vapor Deposition

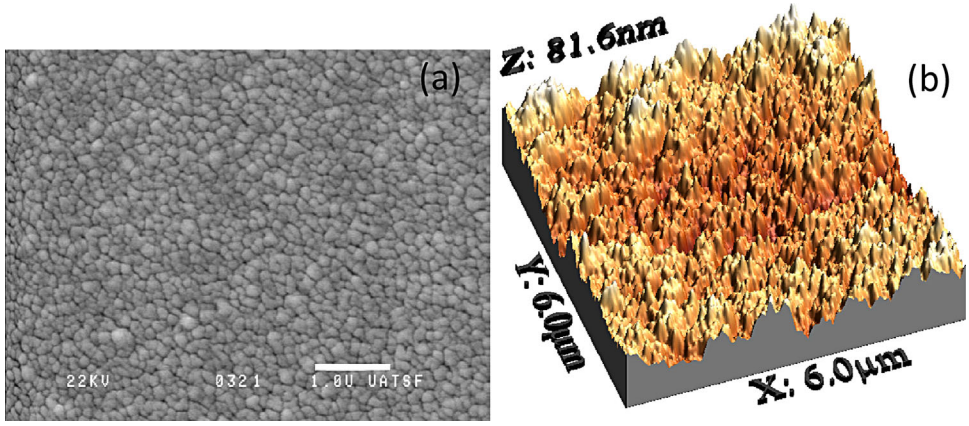

Fig. 3. Images of typical *p*-doped poly-Si samples. a) SEM image; the bar has a length of 1 μm. b) AFM image; the dimensions are indicated on the axes.

while $X_{C,Raman}$ tends to increase for higher boron concentrations. The initial decrease of $X_{C,Raman}$ from ~1 for the intrinsic sample to ~0.75 for the less-doped sample is consistent with the previously discussed decrease of the grain size. Indeed, a lower grain size implies a higher volume proportion of the disordered region between grains, and therefore a lower crystalline fraction. On the other hand, the further increase of the crystalline fraction with boron content observed in Figure 4 may be due to an increase of the crystalline quality caused by the presence of boron acting as nucleation centers.[17] Since we do not observe a variation of the grain size with boron concentration, the effect of boron as an inductor of crystallization prevails, and therefore the crystalline fraction increases. In the literature[21] it is also reported that, by depositing B-doped Si films by low pressure (LP)CVD from SiH_4 and BCl_3, amorphous silicon is obtained for the lowest ratios of boron to silicon atoms in the gas phase, whereas poly-Si films are produced for the intermediate values, changing to amorphous silicon again for the highest concentrations of doping atoms in the gas phase.

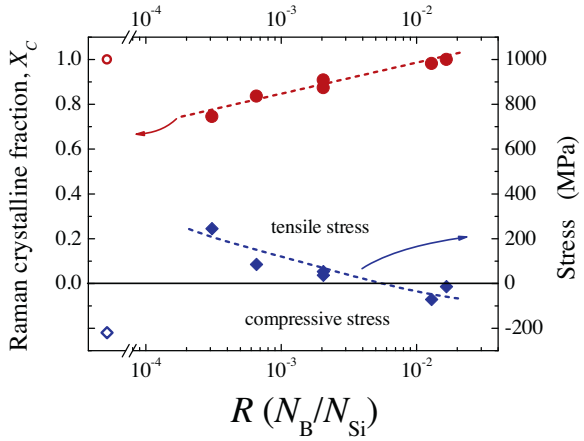

Fig. 4. Raman crystalline fraction (circles, left scale) and stress in the films (diamonds, right scale) as a function of the ratio of boron to silicon atoms in the gas phase. Open symbols correspond to the nominally intrinsic sample. The lines are guides to the eye.

As shown in the literature,[22,23] RS can also be used to estimate the stress present in polycrystalline silicon samples. For the case of in-plane stress, the formula is given by Equation 2.

$$\sigma[\mathrm{MPa}] = -250\Delta\omega[\mathrm{cm}^{-1}] \quad (2)$$

$\Delta\omega = \omega_s - \omega_0$, ω_0 being the wave number of the peak in a stress-free single crystal and ω_s the wave number measured for the stressed sample. In this formula, a negative value corresponds to a compressive stress and a positive value to a tensile stress. The result is shown in Figure 4 (blue diamonds, right scale). The intrinsic samples are in compressive stress (around −200 MPa), as we have found previously.[8] The less-doped samples are in tensile stress, the value for the least-doped sample (245 MPa) being the highest of the series of samples. The stress tends to reduce as doping increases, turning into a compressive stress for the highly doped samples.

We ascribe the compression stress found in the intrinsic samples to a different thermal expansion coefficient between substrate and film. In particular, in our samples, the thermal expansion coefficient of the film is lower than that of the substrate in at least part of the range from the deposition temperature to ambient temperature. Due to this, after the deposition and as the sample cools, the substrate contracts in a greater proportion than the film, causing the compressive stress. On the other hand, it is known that, in some cases of deposition of thin films with columnar structure, the film may grow in such a way that narrow voids form between the columns. Since some atoms establish loose long-range bonds between the columns, a tensile stress develops in those films.[24] In the less-doped samples, these voids may be the cause for the tensile stress observed, and they are an indication of lower-quality films. In these samples, the highest tensile stresses are accompanied by the highest amorphous content, as observed in the Raman spectra. When boron doping increases, stress decreases, suggesting that the voids content also decreases

together with the amorphous content. The compression stresses found in the highly doped samples indicate that their voids content is low, and therefore a thermal expansion-related compressive stress dominates.

The UV reflectance spectrum of crystalline silicon is characterized by two prominent peaks, located at ~280 nm (R_1) and ~365 nm (R_2), corresponding to the optical interband transitions at the X point and along the Γ-L axis of the Brillouin zone, respectively.[25] This UV reflectance spectrum can be used to evaluate the crystalline fraction of a sample, applying the formula given in Equation 3.

$$X_{C,\,UV} = \frac{R_1 - R_2}{R_1^{c-Si} - R_2^{c-Si}} \tag{3}$$

The superscript "c-Si" refers to the values for single crystalline silicon. The results that we have obtained for the series of boron-doped samples are shown in Figure 5a. As can be seen, for the low doping concentrations there is a decrease from the value corresponding to the intrinsic sample ($X_{C,UV} = 0.81$), but for higher boron concentrations $X_{C,UV}$ increases and even surpasses that value. This behavior is consistent with what we have found from the Raman spectra, and can be interpreted as an amorphization of the material for low doping concentrations, and a progressive increase in crystallinity for high doping concentrations.

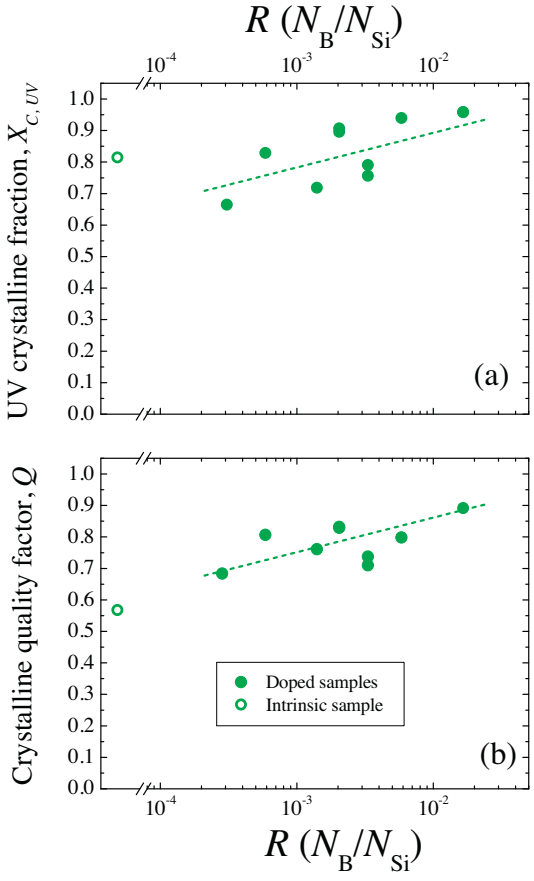

Fig. 5. a) UV crystalline fraction, and b) crystalline quality factor (as functions of R). The first point to the left of each figure corresponds to the nominally intrinsic sample. The lines are a guide to the eye.

The UV reflectance spectra can also be used to estimate the crystalline quality factor (Q) of the poly-Si films. The crystalline quality factor is defined as in Equation 4.[26]

$$Q = \frac{1}{2}\left[\frac{R_1}{R_1^{c-Si}} + \frac{R_2}{R_2^{c-Si}}\right] \tag{4}$$

As discussed in the literature,[26] this factor quantifies how similar to the spectrum of single crystalline silicon is that of each sample. The results that we have found for the series of samples are shown in Figure 5b. For the doped samples Q takes values close to those of $X_{C,UV}$, and also exhibits a growing trend with R. On the other hand, for the intrinsic sample we have $Q = 0.57$ while $X_{C,UV} = 0.81$. This discrepancy is probably due to the influence of the surface roughness on the calculation of Q. Surface roughness reduces the amplitude of both peaks, thus decreasing the crystalline quality factor. The fact that Q is similar to $X_{C,UV}$ for the doped samples seems to indicate that the roughness is lower in these samples than in the intrinsic ones. This point is confirmed by AFM measurements (Fig. 3b), which give an rms roughness of ~11 nm for a doped sample and ~46 nm for the intrinsic sample, both being of approximately the same thickness.

XRD was used to evaluate the crystalline orientation of the poly-Si films. For all the deposition conditions used, we have found a clear preferential orientation with the (220) plane parallel to the sample surface (Fig. 6a).

To quantify the degree of preferential orientation of the films, we have calculated the orientation factor α_{hkl}, defined by the formula given in Equation 5.[27]

$$\alpha_{hkl} = \frac{(I_{hkl}/I_{0,hkl})}{\sum_{hkl}(I_{hkl}/I_{0,hkl})} \times 100 \tag{5}$$

I_{hkl} is the measured intensity for the (hkl) plane, and $I_{0,hkl}$ is the intensity of the corresponding Si powder diffraction peak used as a standard reference. This factor quantifies the volume fraction of grains with the specified orientation. The orientation factor is presented in Figure 7 as a function of R. As can be seen, the intrinsic sample shows an almost 100% preferential (220) orientation. On the other hand, for the compensated sample the degree of (220) orientation is reduced to ≈65%. The preferential (220) orientation increases again with the boron concentration, reaching values close to 100% for the heavily boron-doped samples. This behavior is consistent with the results found for the UV and Raman crystalline fractions. The preferential (220) orientation of the layers is usually associated with the growth of columnar grains, and with a low recombination activity at the grain boundaries. The (220) texture ensures

Chemical Vapor Deposition

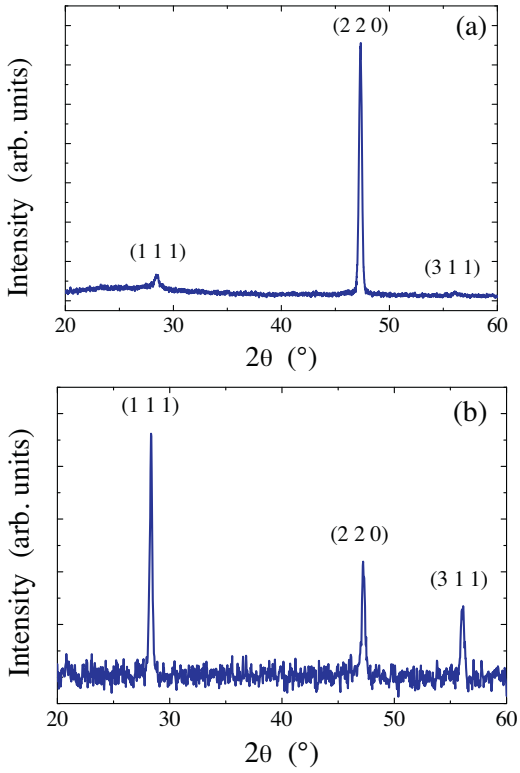

Fig. 6. XRD spectra of thin poly-Si films. a) Typical *p*-doped sample, where a preferential (220) orientation can be seen. b) n^+-doped sample deposited at a temperature of 850 °C, where the relation of the peak intensities is consistent with a random orientation of the crystalline grains.

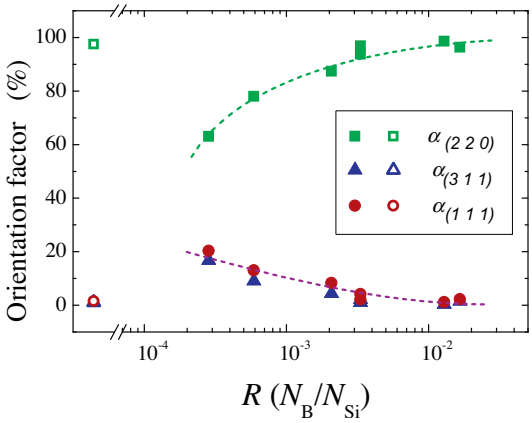

Fig. 7. Orientation factor as a function of *R*. The first points to the left correspond to the nominally intrinsic sample. The lines are guides to the eye.

that many grain boundaries should be of the [110]-tilt type, which are electrically inactive and grow without broken bonds.[28] Therefore, the disordered inter-grains region should be reduced, and the crystallinity should increase, as measured from UV reflectance and RS. The growth of poly-Si with a preferential (220) orientation on different substrates is also mentioned in several publications,[18,27,29] although a degree of orientation as high as the one obtained here has only been obtained utilizing dichlorosilane.[30] The

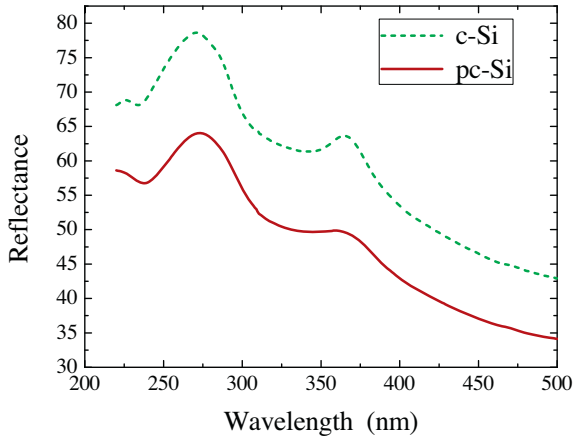

Fig. 8. Reflectance spectra in the UV region of a crystalline silicon wafer and a thin poly-Si (n^+) film deposited on glass.

columnar structure and the preferential (220) orientation of the films are both favorable characteristics for photovoltaic applications.

2.2. Phosphorus-doped Samples

The XRD spectra of a n^+ poly-Si thin film deposited on glass exhibit the crystalline peaks corresponding to the (111), (220), and (311) planes with an intensity relation very close to that of a powder sample (Fig. 6b). This means that the polycrystalline structure does not exhibit any preferential orientation, in contrast to the results found on intrinsic and *p*-doped materials which grew strongly (220)-oriented. Sarret et al.[31] also found that large phosphorus concentrations tend to suppress any preferential orientation in their polycrystalline samples deposited by LPCVD. The lack of preferential orientation can also be associated with the absence of a columnar structure on the films, which was confirmed by SEM observations of the sample cross-sections.

The reflectance spectrum of a typical n^+ poly-Si sample is shown in Figure 8, together with the spectrum of a polished c-Si wafer. Both spectra exhibit a similar aspect, except for a displacement of the poly-Si spectrum towards lower reflectance values. This measurement disproves the presence of an amorphous phase and confirms the polycrystalline nature of the material. The reason for this shift is probably the high roughness of the film, which reduces the reflectance for the complete spectrum. The crystalline fraction of this sample, calculated from Equation 3, results in the value $X_{C,UV} = 0.95$, confirming the high crystallinity of the sample.

Figure 9 shows the Raman spectra of a n^+ poly-Si sample and of a c-Si wafer. As can be seen, the peak of the polycrystalline sample is wider and is shifted towards lower energies. The full width at half maximum (FWHM) of the Raman peak has been correlated with the grain size,

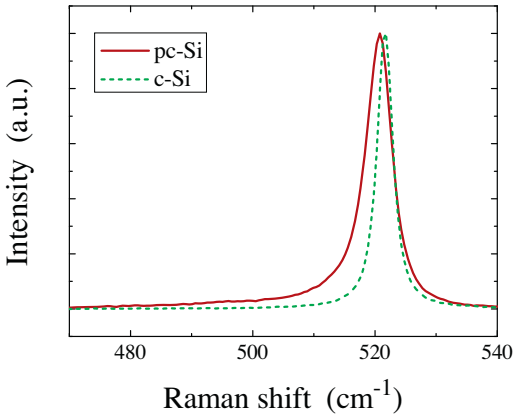

Fig. 9. Raman spectra of a n^+ polycrystalline silicon sample and of a c-Si wafer.

although a precise determination is not possible.[32] In Figure 9, the FWHM of the float zone monocrystalline Si wafer is 3.0 cm^{-1}, while that of the poly-Si sample is 5.0 cm^{-1}. This is an indication of a relatively large grain size. Moreover, no signal of an amorphous component at 480 cm^{-1} can be seen, confirming the truly polycrystalline nature of this material. The Raman crystalline fraction, calculated from Equation 1, results in a value $X_{C,\ Raman} \approx 0.92$ for all the samples, in agreement with the results from UV reflectance. The stress of the films, evaluated from Equation 2, results in a tensile stress of around 200 MPa. Other authors have also found tensile stresses in P-doped samples.[33]

Measurements of electrical conductivity as a function of temperature show a metallic behavior of the heavily doped samples, with a room temperature dark conductivity of around 950 $\Omega^{-1}\,cm^{-1}$. Hall effect measurements confirm the *n*-type character of the samples, with an electron concentration of $\sim 3 \times 10^{20}$ cm^{-3} and a Hall mobility of $\sim$20 $cm^2\,V^{-1}\,s^{-1}$. This mobility is approximately 3.5 times lower than the mobility of c-Si doped with the same phosphorus concentration. The reduction in mobility for the poly-Si samples is probably due to scattering at grain boundaries, and with charges trapped at defect states. As we have mentioned, the phenomenon of charge trapping also occurs in *p*-doped poly-Si thin films, and consists in part of the free carriers getting immobilized at the defect states located at the grain boundaries. In this way, a potential barrier is formed which opposes the movement of the free carriers, reducing its mobility.[14] The results obtained however, are good enough and suggest that the material is suitable for the n^+ layer of a solar cell.

2.3. Solar Cells

Conventional c-Si cells are typically produced through phosphorus diffusion on a *p*-type wafer to form the emitter. The process is relatively slow (approximately 50 min) and involves stages at temperatures of the order of 950 °C, resulting in a concentration profile of the Gaussian type (or complementary error function) with its maximum at the front surface. The process requires carrying out cleaning steps to the wafers, both before and after the diffusion. On the contrary, the deposition of the emitter by CVD takes only some minutes and can be done at temperatures (as in the case of this work) of the order of 810 °C. Furthermore, it provides the possibility of designing the concentration profile, and needs fewer etching steps since no silicate glass is formed after the diffusion. For these reasons, the deposition of the emitter by CVD for c-Si solar cells is a process with potential to achieve a cost reduction and an increase in the efficiency.

We deposited c-Si (*p*)/poly-Si (n^+) heterojunctions, where the substrates are boron-doped c-Si wafers. Figure 10 shows the *J* - *V* curves, measured in darkness and under AM 1.5 solar illumination, of a cell for which the thickness of the n^+ poly-Si layer is 130 nm. The illuminated curve was measured at the equilibrium temperature under light (around 58 °C), which reduces the series resistance and causes the curves to cross. In any case, the measurements show the presence of a high series resistance (specific series resistance of $\sim$2 $\Omega\,cm^2$), evidence of an inefficient contact scheme, which deteriorates the fill factor ($F = 0.58$), however the values obtained for the open circuit voltage (up to 507 mV for other cells, not shown here) and the short-circuit current density (up to 29.6 mA cm^{-2}) indicate the presence of a good junction between the materials, which can lead to good solar cells. The efficiencies of $\sim$8% obtained in these preliminary experiments, without optimizing the series resistance and with no surface passivation, are encouraging results. For comparison, the values corresponding to poly-Si solar cells on glass produced by the company CSG Solar[34] were $V_{OC} = 492$ mV, $J_{SC} = 29.7$ mA cm^{-2}, FF = 0.721, $\eta = 10.5\%$; while the parameters for

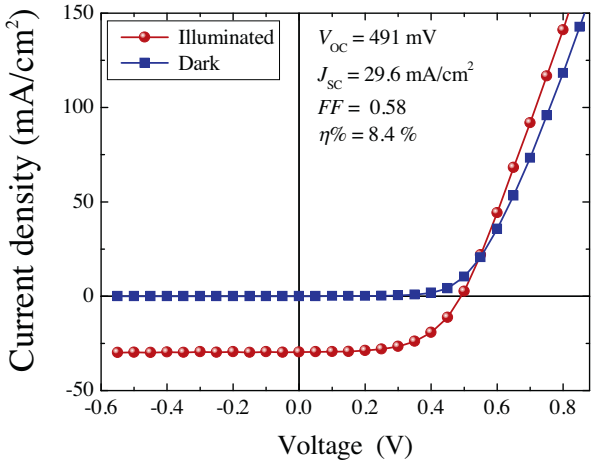

Fig. 10. *J-V* curve of a c-Si (*p*)/poly-Si (n^+) solar cell in the dark, and under illumination. A large series resistance degrades the fill factor, but the open-circuit voltage and short-circuit current have reasonable values, giving a conversion efficiency of around 8.4%.

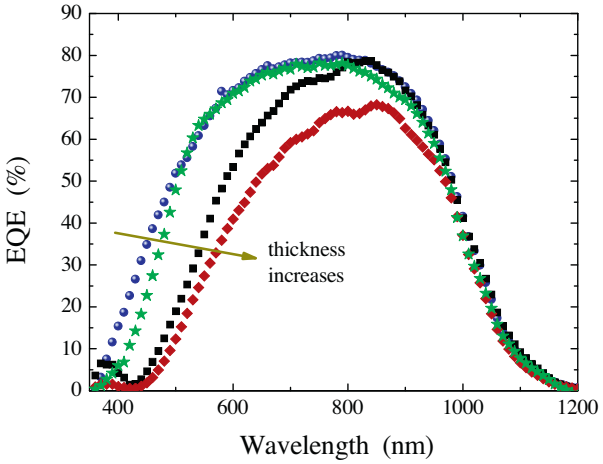

Fig. 11. EQEs of c-Si (p)/poly-Si (n^+) solar cells with various thicknesses of the n^+ layer. The response in the blue region decreases with the increase of the n^+ layer thickness.

the record-efficiency c-Si solar cell are $V_{OC} = 706\,mV, J_{SC} = 42.7\,mA\,cm^{-2}$, FF = 0.828, $\eta = 25.0\%$.[35] Moreover, the external quantum efficiency (EQE) measurements (see Fig. 11) reveal a quite wide response, similar to that of conventional c-Si solar cells. The thickness of the n^+ layer has a clear effect on the EQE, with a noticeable decrease of the blue response with the increase of the emitter thickness. This is clearly due to an increase in light absorption in this highly defective layer, where a high recombination causes the loss of the generated carriers.

3. Conclusion

In this work, we present results of the deposition of boron- and phosphorus-doped polycrystalline silicon thin films on glass and crystalline silicon substrates. The precursor gas (TCS), the doping agents (BBr_3 and PCl_3), and the substrate (aluminosilicate glass), all of low cost, proved to be adequate for silicon deposition by APCVD at intermediate temperatures. The p-doped films exhibited a strong (220)-preferred orientation, indicative of grain boundaries of low recombination activity. On the contrary, the n-doped samples did not show any preferential orientation, nor did they exhibit columnar structure. In all cases, a high crystalline fraction could be obtained with a reasonable value for the carrier's mobility. The whole range of doping conditions – heavily n-type, compensated, slightly p-type, and clearly p-type – could be obtained by varying the BBr_3 and PCl_3 concentrations in the gas phase.

Our results demonstrate the feasibility of directly depositing polycrystalline silicon thin film solar cells on glass substrates by APCVD at intermediate temperatures. Heterojunction poly-Si/c-Si solar cells were produced using n^+ poly-Si thin films. These devices can be more convenient than conventional diffused cells from the point of view of cost and efficiency due to a number of advantages of the CVD process. High values were measured for the open-circuit voltage (up to 507 mV) and the short-circuit current (up to 29.6 mA cm^{-2}). The thinnest n^+ layer proved to be the most suitable to make use of the solar spectrum, however the series resistance was high and the fill factor was low, implying that the metal/semiconductor contacts still have to be improved. When this is achieved, the efficiency obtained – 8.4% maximum up to now – will certainly increase.

4. Experimental

The CVD reactor that we used was a batch-type, hot-wall reactor, consisting of a horizontal quartz tube located inside a tubular oven. Sheets of Schott AF37 glass were used as substrates, heated to a temperature of 850 °C. The substrates were 25 mm × 8 mm in size, and 1 mm thick. The precursor compound was TCS, and hydrogen was used as carrier and reaction gas. A constant flow of 60 sccm of hydrogen was made to bubble in liquid TCS, the temperature of which was kept at 0 °C. The dopant sources should be reactants that adapt to the APCVD process. We chose liquid boron tribromide (BBr_3) as a B source and liquid phosphorous trichloride (PCl_3) as a P source. These compounds were carried into the reaction chamber by making a hydrogen flow of 3 to 5 sccm bubble into the liquids. The partial pressure of BBr_3 was controlled by adjusting its temperature between -35 and +30 °C, and therefore the proportion of boron in the samples was varied. On the other hand, PCl_3 was kept at a temperature of 0 °C, adjusting the hydrogen flow.

The thickness of the films was determined by measurements of the reflectance spectra in the visible-near IR region. Samples were structurally characterized by SEM, AFM, reflectance spectroscopy in the UV-vis region, XRD, and RS. SEM and EPMA were performed with a JEOL JSM-35C microscope equipped with an energy-dispersive spectrometry (EDS) system. AFM images were taken with an AFM NANOTEC system operated in tapping mode. Reflectance spectroscopy in the UV-vis region was performed in a Shimadzu 3600 spectrometer provided with an integrating sphere. Samples were etched in a diluted HF solution prior to the reflectance measurements to remove the native oxide. XRD was carried on in a Shimadzu XD-D1 diffractometer in a θ-2θ configuration. For RS we used a Witec Alpha R300 micro-Raman system operating at a wavelength of 532 nm from a solid-state laser. The spot size was about 1 μm and the laser power was 0.72 mW.

Evaporated electrodes were deposited on top of the samples for electrical contacts, disposed in a coplanar geometry with a separation of 1 mm between them (for conductivity measurements), or at the edges of the square samples in the van der Pauw configuration (for Hall effect measurements). Aluminum was used for the p-doped samples and silver for the n-doped samples. The samples were annealed at 300 °C for 30 min after the evaporation of the contacts, and the ohmicity of the contacts after the thermal treatment was verified. Dark conductivity was measured as a function of temperature between 160 and 25 °C, placing the samples inside a cryostat evacuated to a base pressure of ~10^{-6} Torr. Activation energy was calculated from an Arrhenius plot, assuming an activated behavior. Hall effect measurements were performed using a magnetic field of 0.65 T.

Solar cells were produced by depositing poly-Si (n^+) on boron-doped silicon wafers with (100) orientation and a resistivity of ~5 Ω cm. For these samples, the size of the substrates was also 25 mm × 8 mm, with a thickness of about 0.7 mm. The deposition temperature in this case was 810 °C. After the deposition of the poly-Si film and before the deposition of the contacts, these samples were cut into pieces of about 7 mm × 7 mm. Contacts were deposited on each piece by evaporation of aluminum on the p-type wafer and of gold on the n^+ layer. The cells were annealed at 300 °C for 30 min after the deposition of the Al contact and before the deposition of the Au contact. The area of the cells was about 0.5 cm^2. The current density - voltage (J-V) curve of the cells was measured at room temperature in dark conditions, and under AM 1.5 sunlight illumination. The EQE of the devices was measured at room temperature, using as light source a 50 W tungsten-halogen lamp and chopping the light beam. A lock-in amplifier SR530, a current amplifier SR570, and a chopper controller SR540 were used, all of them made by Stanford Research Systems. The measurements performed on the cells were

carried out shortly after the deposition of the Au contact to avoid the deterioration of the devices due to the fast diffusion of gold in silicon.

[1] G. Beaucarne, S. Bourdais, A. Slaoui, J. Poortmans, *Thin Solid Films* **2002**, *403–404*, 229.
[2] S. Reber, T. Kieliba, S. Bau, in Thin Film Solar Cells Fabrication. Characterization and Applications (Eds.J. Poortmans, V. Arkhipov), Wiley, Chichester, **2006**.
[3] SCHOTT Displayglass Jena GmbH, Datasheet of glass AF37 (www.schott.com) **2004**.
[4] M. Howe-Grant, J. Kroschwitz, *Kirk-Othmer Encyclopedia of Chemical Technology - Vol 22*, John Wiley & Sons, New York, **1997**.
[5] R. Monna, A. Slaoui, A. Lachiq, J. C. Muller, *Mater. Sci. Eng. B* **1996**, *39*, 48.
[6] Y. Ishikawa, Y. Yamamoto, T. Hatayama, Y. Uraoka, T. Fuyuki, *Sol. Energy Mater. Sol. Cells* **2002**, *74*, 255.
[7] A. G. Benvenuto, R. H. Buitrago, J. A. Schmidt, *Eur. Phys. J. Appl. Phys.* **2012**, *58*, 20101.
[8] A. G. Benvenuto, R. H. Buitrago, A. Bhaduri, C. Longeaud, J. A. Schmidt, *Semicond. Sci. Technol.* **2012**, *27*, 125013.
[9] G. Beaucarne, S. Bourdais, A. Slaoui, J. Poortmans, *Appl. Phys. A* **2004**, *79*, 469.
[10] G. Beaucarne, I. Gordon, D. Van Gestel, L. Carnel, J. Poortmans, in *Proc. 21st Eur. Photovoltaic Sol. Energy Conf. Vol I* (Eds: J. Poortmans, H. Ossenbrink, E. Dunlop, P. Helm), WIP, Munich **2006**, p.721.
[11] B. Rau, I. Sieber, B. Selle, S. Brehme, U. Knipper, S. Gall, W. Fuhs, *Thin Solid Films* **2004**, *451–452*, 644.
[12] H. J. Queisser, E. E. Haller, *Science* **1998**, *281*, 945.
[13] D. Angermeier, R. Monna, A. Slaoui, J. C. Muller, *J. Cryst. Growth* **1998**, *191*, 386.
[14] J. Y. W. Seto, *J. Appl. Phys.* **1975**, *46*, 5247.
[15] P. Münster, M. Sarret, T. Mohammed-Brahim, N. Coulon, J. Y. Mevellec, *Phil. Mag. B* **2002**, *82*, 1695.
[16] G. Baccarani, B. Riccò, G. Spadini, *J. Appl. Phys.* **1978**, *49*, 5565.
[17] T. Toyama, W. Yoshida, Y. Sobajima, H. Okamoto, *J. Non-Cryst. Solids* **2008**, *354*, 2204.
[18] A. Slaoui, R. Monna, D. Angermeier, S. Bourdais, J. C. Muller, in *Proc. 26th IEEE Photovoltaic Specialists Conf.* (Eds: P. Basore), IEEE, Anaheim **1997**, p 627.
[19] L. Carnel, I. Gordon, D. Van Gestel, G. Beaucarne, J. Poortmans, A. Stesmans, *J. Appl. Phys.* **2006**, *100*, 0637021.
[20] A. T. Voutsas, M. K. Hatalis, J. Boyce, A. Chiang, *J. Appl. Phys.* **1995**, *78*, 6999.
[21] B. Caussat, E. Scheid, B. de Mauduit, R. Berjoan, *Thin Solid Films* **2004**, *446*, 218.
[22] I. De Wolf, *Semicond. Sci. Technol.* **1996**, *11*, 139.
[23] V. Paillard, P. Puech, R. Sirvin, S. Hamma, P. Roca i Cabarrocas, *J. Appl. Phys.* **2001**, *90*, 3276.
[24] A. Rockett, *The Materials Science of Semiconductors*, Springer, New York **2008**.
[25] G. Harbeke, L. Jastrzebski, *J. Electrochem. Soc.* **1990**, *137*, 696.
[26] A. Straub, P. I. Widenborg, A. Sproul, Y. Huang, N. Harder, A. G. Aberle, *J. Cryst. Growth* **2004**, *265*, 168.
[27] D. Angermeier, R. Monna, S. Bourdais, A. Slaoui, J. C. Muller, *Prog. Photovolt. Res. Appl.* **1998**, *6*, 219.
[28] J. H. Werner, R. Dassow, T. J. Rinke, J. R. Kohler, R. B. Bergmann, *Thin Solid Films* **2001**, *383*, 95.
[29] S. Bourdais, G. Beaucarne, J. Poortmans, A. Slaoui, *Physica B* **1999**, *273–274*, 544.
[30] Y. Ishikawa, Y. Yamamoto, T. Hatayama, Y. Uraoka, T. Fuyuki, *Sol. Energy Mater. Sol. Cells* **2002**, *74*, 255.
[31] M. Sarret, A. Liba, O. Bonnaud, F. L. Bihan, B. Fortin, *J. Phys. IV* **1993**, *3*, 411.
[32] C. Becker, F. Ruske, T. Sontheimer, B. Gorka, U. Bloeck, S. Gall, B. Rech, *J. Appl. Phys.* **2009**, *106*, 084506.
[33] W. Wei, *Vacuum* **2007**, *81*, 857.
[34] S. Gall, B. Rech, *Sol. Energy Mater. Sol. Cells* **2003**, *119*, 306.
[35] M. A. Green, K. Emery, Y. Hishikawa, W. Warta, *Prog. Photovolt.: Res. Appl.* **2010**, *18*, 346.

